Sample Zone Dynamics in Peak Mode Isotachophoresis

Tarun K. Khurana and Juan G. Santiago*

Department of Mechanical Engineering, Stanford University, 440 Escondido Mall, Building 530, Room 225, Stanford, California 94305

We present a theoretical and experimental study of analyte preconcentration via peak mode isotachophoresis (ITP). We perform perturbation analysis of the governing equations that includes electromigration, diffusion, buffer reactions, and nonlinear ionic strength effects. This analysis relaxes the inherent numerical stiffness and achieves a fast solution to the transient sample evolution problem. In this model, we have incorporated a semiempirical relation to capture dispersion phenomenon within ITP interfaces. We also present a simple, closed-form analytical model that identifies key parameters governing the preconcentration dynamics in peak mode ITP. We have validated our models through a detailed experimental study performed in constant current conditions. The relevant governing experiment parameters were varied independently; namely, the leading electrolyte concentration, trailing electrolyte concentration, and current. Through our experimental study, we have identified optimum conditions to achieve high preconcentration ratio and sample accumulation rates. Our approach to the theoretical problem and experimental study provides useful guidelines in optimizing parameters such as detector location, ITP duration, and electrolyte composition in ITP preconcentration and separation assays.

On-chip capillary electrophoresis has evolved as a chemical and biological analysis technology of choice in a variety of applications and offers the potential of parallel, high-throughput assays with low reagent volumes.[1,2] However, smaller sample volume and shallow channel depth in planar wet-etched microfluidic devices can result in lower sensitivity due to shorter optical path length. Hence preconcentration techniques are often required to improve sample loading and detection sensitivity.[3]

A number of electrokinetic preconcentration techniques exist and have been reviewed extensively.[3–5] These are classified as focusing techniques if the drift velocity of ions reduces and changes sign across the focus point (e.g., allowing analyte zones to reach steady state) and as stacking techniques if the drift velocity reduces but does not change sign.[6] Common stacking methods include field-amplified sample stacking (FASS),[7] field-amplified sample injection,[8] and pH mediated stacking; [9] and focusing techniques include isoelectric focusing (IEF),[10] temperature gradient focusing (TGF),[11] and electric field gradient focusing.[12] Isotachophoresis (ITP) remains a popular preconcentration technique for on-chip electrophoresis due to its robustness, ubiquity, and ease of implementation.[13] Like other focusing techniques, it offers inherent preconcentration effects that counter dispersion and offers selective (mobility based) preconcentration.

In the simplest version of ITP, analytes segregate into distinct zones characterized by a plateau shape at steady state.[14] For strong, univalent electrolytes, composition of these plateau zones can be estimated using the Kohlrausch regulating function (KRF).[15] Analogous conservation laws exist for weak electrolytes.[16,17] However, such analyses are not applicable to typical ITP preconcentration as trace analytes rarely form plateau zones. For typical cases involving trace analytes, ITP zone widths are on the order of the interface width of adjacent zones.[18,19] The latter ITP regime has been called the peak mode[20] or spike mode[21] where the focused analyte concentration profile is approximately Gaussian.[22] Unlike the plateau mode, sample zone shapes in peak mode ITP are governed by the electric field gradient and dispersion at the leading−trailing (LE−TE) boundary.[23] Here, application of KRF theory (or similar models for plateau ITP) can be highly inaccurate; for example, KRF can overpredict analyte concentration by 5 or more orders of magnitude.[24]

* To whom correspondence should be addressed. E-mail: juan.santiago@stanford.edu. Fax: (650) 723-7657.

(1) Jacobson, S.; Hergenroder, R.; Koutny, L.; Ramsey, J. *Anal. Chem.* **1994**, *66*, 1114–1118.
(2) Dolník, V.; Liu, S.; Jovanovich, S. *Electrophoresis* **2000**, *21*, 41–54.
(3) Chien, R. *Electrophoresis* **2003**, *24*, 486–497.
(4) Breadmore, M. C.; Haddad, P. R. *Electrophoresis* **2001**, *22*, 2464–2489.
(5) Osbourn, D. M.; Weiss, D. J.; Lunte, C. E. *Electrophoresis* **2000**, *21*, 2768–2779.
(6) Ivory, C. F. *Sep. Sci. Technol.* **2000**, *35*, 1777–1793.
(7) Burgi, D. S.; Chien, R. L *Anal. Chem.* **1991**, *63*, 2042–2047.
(8) Jackson, P. E.; Haddad, P. R. *TrAC, Trends Anal. Chem.* **1993**, *12*, 231–238.
(9) Zhao, Y. P.; Lunte, C. E. *Anal. Chem.* **1999**, *71*, 3985–3991.
(10) Herr, A. E.; Molho, J. I.; Drouvalakis, K. A.; Mikkelsen, J. C.; Utz, P. J.; Santiago, J. G.; Kenny, T. W. *Anal. Chem.* **2003**, 75.
(11) Ross, D.; Locascio, L. E. *Anal. Chem.* **2002**, *74*, 2556–2564.
(12) Koegler, W. S.; Ivory, C. F. *J. Chromatogr., A* **1996**, *726*, 229–236.
(13) Bocek, P.; Deml, M.; Gebauer, P.; Dolnik, V. *Analytical Isotachophoresis* ; VCH: New York, 1988.
(14) Martin, A. J. P.; Everaerts, F. M. *Anal. Chim. Acta* **1967**, *38*, 233–237.
(15) Kohlrausch, F. *Ann. Phys. Chem.* **1897**, *298*, 209–239.
(16) Alberty, R. A. *J. Am. Chem. Soc.* **1950**, *72*, 2361–2367.
(17) Jovin, T. M. *Biochemistry* **1973**, *12*, 871–879.
(18) Svoboda, M.; Vacik, J. *J. Chromatogr., A* **1976**, *119*, 539–547.
(19) Gebauer, P.; Bocek, P. *Electrophoresis* **1995**, *16*, 1999–2007.
(20) Chen, S.; Graves, S. W.; Lee, M. L. *J. Microcol. Sep.* **1999**, *11*, 341–345.
(21) Nagyova, I.; Kaniansky, D. *J. Chromatogr., A* **2001**, *916*, 191–200.
(22) Khurana, T. K.; Santiago, J. G. *Anal. Chem.* **2008**, *80*, 279–286.
(23) Gebauer, P.; Bocek, P. *Electrophoresis* **1995**, *16*, 1999–2007.
(24) Jung, B.; Bharadwaj, R.; Santiago, J. G. *Anal. Chem.* **2006**, *78*, 2319–2327.

10.1021/ac800792g CCC: $40.75
Published on Web 07/22/2008

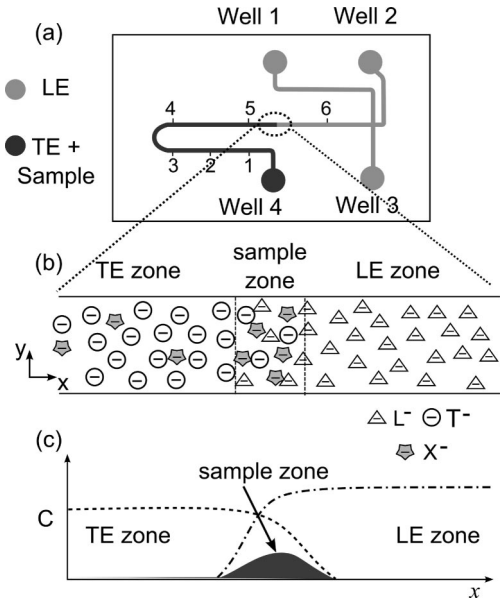

Figure 1. Schematic of a typical single interface ITP experiment. An interface between LE and TE is set up at the entrance of well 4, and high voltage is applied across well 2 and 4 to initiate ITP preconcentration. Schematics b and c show the distribution and concentration profile of the leading, trailing, and sample ions across the LE−TE interface after initiating ITP. Also shown are six detection regions (numbered 1−6) located 4.5, 9.5, 13.5, 21, 31, and 41 mm downstream of the TE well, respectively.

In this paper, we describe the theoretical and experimental study of the transient sample preconcentration in peak mode ITP. We present a numerical solution to the area averaged equations for species transport and employ regular perturbation analysis to reduce the numerical stiffness and simplify the solution. We use a semiempirical estimate of dispersion coefficient which captures trends in zone shape and sample peak concentration. We also present a simple 1D analytical model for estimating the analyte accumulation rate and preconcentration ratio. The latter identifies key experiment parameters that govern the dynamics. We also performed an experimental parametric study of ITP preconcentration (in constant current mode) which isolates the effect of the governing parameters. The study validates the models and provides a guide to experimental design and optimization of practical ITP assays.

THEORY

Qualitative Assay Description. In ITP preconcentration experiments, the sample species are added to the trailing electrolyte (TE) to improve sample loading and avoid unusually high electroosmotic flow (EOF) that can occur in the hydrodynamic injections of the sample zone.[24,25] An initial interface between the leading (LE) and TE is established as shown schematically in Figure 1. When an electric field is applied, sample ions overspeed the slow trailing ions and accumulate at the migrating LE−TE interface. Because of the low concentration of sample ions in the TE zone compared to other background ions (typically ~1000-fold or more lower), the LE and TE boundaries move at nearly identical speed as in typical ITP.

Perturbation Analysis for Peak Mode ITP Preconcentration Dynamics. A generalized model for the transport of electrolyte species requires modeling of acid−base equilibrium reactions[26,27] and the ionic strength dependence of species mobility and activity. Gas et al.[28] presented such an electromigration model, and these effects are included in the electrophoresis software SIMUL 5 available for free use.[29] However, these models have limited application to the peak-mode ITP problem due to the inherent numerical stiffness that results in numerical oscillations in the solution. Also, these models do not account for interface dispersion due to nonuniform EOF which strongly influences zone width. The current model addresses these shortcomings by relaxing the numerical stiffness of the problem using perturbation analysis and incorporating a semiempirical dispersion model.

For a dilute electrolyte solution, the general advection diffusion equation for a species i, possessing multivalent states is given by

$$\frac{\partial C_i}{\partial t} + \boldsymbol{u_b}\cdot\nabla C_i = \nabla\cdot\sum_{z=z_1}^{z_n}(-\mu_{i,z}C_{i,z}\boldsymbol{E} + D_{i,z}\nabla C_{i,z}) \qquad (1)$$

where C_i is the total concentration of species i, E is the electric field, and $\boldsymbol{u_b}$ is the bulk velocity due to pressure driven and electroosmotic flow (EOF). Here, $C_{i,z}$ is the concentration, $D_{i,z}$ is the diffusion coefficient, $\mu_{i,z}$ is the electrophoretic mobility, and z is the valence of the zth charge state of species i. The concentration of the zth charge state of species i is related to the $(z-1)$th charge state by the respective acid−base equilibrium reaction constants.

The electric field distribution can be solved for from the current conservation equation[28]

$$\boldsymbol{E} = \frac{j}{\sigma} - \frac{F}{\sigma}\left(\sum_i\sum_{z=z_1}^{z_n} zD_{i,z}\nabla C_{i,z}\right) \qquad (2)$$

where σ is the conductivity of the electrolyte defined by $\sigma = \sum_i\sum_{z=z_1}^{z_n} zF\mu_{i,z}C_{i,z}$

The simple ITP preconcentration system, shown in Figure 1, consists of four electrolyte species: leading ion (L), trailing ion (T), counterion (C), and sample species (S). In applications of ITP to trace analytes, even focused sample concentration is much smaller than the background ion concentration[24,30] (here 10−100 μM stacked sample concentration versus 10−100 mM background ion concentration). In this regime, sample ions have negligible contribution to the development of a local electric field and background ion concentration. We show this formally by performing regular perturbation analysis, treating the ratio of sample concentration to leading electrolyte concentration as the smallness parameter $\varepsilon = C_S/C_L$.

The dependent variables, namely, species concentrations and electric field are expanded in terms of ε as $Y_i = Y_i^0 + \varepsilon Y_i^1 + \varepsilon^2 Y_i^2 + \ldots$, where ϵ is the jth order term of variable Y_i. We expand the

(25) Xu, Z. Q.; Nishine, T.; Arai, A.; Hirokawa, T. *Electrophoresis* **2004**, *25*, 3875–3881.
(26) Bier, M.; Palusinski, O. A.; Mosher, R. A.; Saville, D. A. *Science* **1983**, *219*, 1281–1287.
(27) Ermakov, S. V.; Mazhorova, O. S.; Zhukov, M. Y. *Electrophoresis* **1992**, *13*, 838–848.
(28) Hruska, V.; Jaros, M.; Gas, B. *Electrophoresis* **2006**, *27*, 984–991.
(29) http://www.natur.cuni.cz/gas/.
(30) Jung, B.; Zhu, Y.; Santiago, J. G. *Anal. Chem.* **2007**, *79*, 345–349.

variables of eq 1 and 2 and compare terms with identical powers of ϵ in the resulting equation. The resulting zeroth order equations for the background ions (LE, TE, and counterion) and the electric field are given by

$$\frac{\partial C_i^0}{\partial t} + \boldsymbol{u_b} \cdot \nabla C_i^0 = \nabla \cdot \sum_{z=z_1}^{z_n} (-\mu_{i,z} C_{i,z}^0 \boldsymbol{E^0} + D_{i,z} \nabla C_{i,z}^0) \quad (3)$$

The expressions for E^0 and σ^0 are same as those in eq 2 with concentration term $C_{i,z}$ replaced by $C_{i,z}^0$.

For the sample ion concentration, we obtain simply $C_S^0 = 0$ as the zeroth order term, and for the first order term

$$\frac{\partial C_S^1}{\partial t} + \boldsymbol{u_b} \cdot \nabla C_S^1 = \nabla \cdot \sum_{z=z_1}^{z_n} (-\mu_{S,z} C_{S,z}^1 \boldsymbol{E^0} + D_{S,z} \nabla C_{S,z}^1) \quad (4)$$

We infer two important results from this which helps us simplify the solution: (a) The zeroth order equations for background species and electric field do not depend on the sample ion concentration. (b) The first order sample concentration depends on the zeroth order electric field distribution.

Next, we perform area-averaging of zeroth order background species concentration and electric field and of first order sample concentration equations to obtain one-dimensional area-averaged species transport equations. The resulting equation for background ions is given by

$$\frac{\partial \langle C_i^0 \rangle}{\partial t} + \langle u_b^0 \rangle \frac{\partial \langle C_i^0 \rangle}{\partial x} = \frac{\partial}{\partial x} \sum_{z=z_1}^{z_n} \left(-\mu_{i,z} \langle C_{i,z}^0 \rangle \langle E^0 \rangle + D_{\text{eff},i,z} \frac{\partial \langle C_{i,z}^0 \rangle}{\partial x} \right) \quad (5)$$

We here lump the dispersion effect due to nonuniform bulk velocity and electric field into an effective dispersion coefficient D_{eff} defined in eq 8. The operator $\langle f(x,y) \rangle$ denotes area-averaging of the variable $f(x,y)$; here this is an integral over the transverse direction, $\langle f(x,y) \rangle = 1 / 2h \int_{-h}^{h} f(x,y)\, dy$.

The area-averaged equations for the zeroth order electric field and for first order sample concentration are

$$\langle E^0 \rangle = \frac{j}{\langle \sigma^0 \rangle} - \frac{F}{\langle \sigma^0 \rangle} \left(\sum_i \sum_z z D_{\text{eff},i,z} \frac{\partial \langle C_{i,z}^0 \rangle}{\partial x} \right) \quad (6)$$

$$\frac{\partial \langle C_S^1 \rangle}{\partial t} + \langle u_b^0 \rangle \frac{\partial \langle C_S^1 \rangle}{\partial x} = \frac{\partial}{\partial x} \sum_{z=z_1}^{z_n} \left(-\mu_{S,z} \langle C_{S,z}^1 \rangle \langle E^0 \rangle + D_{\text{eff},S,z} \frac{\partial \langle C_{S,z}^1 \rangle}{\partial x} \right) \quad (7)$$

Here $\langle \sigma_0 \rangle$ is the area averaged conductivity given by $\langle \sigma^0 \rangle = \sum_i \sum_{z=z_1}^{z_n} zF\mu_{i,z} \langle C_{i,z}^0 \rangle$

The effective dispersion coefficient D_{eff} accounts for axial diffusion and for shearing of the interface due to deviation of concentration and the electric and bulk velocity field from the area-averaged values and is given by

$$D_{\text{eff},i,z} \frac{\partial \langle C_{i,z}^0 \rangle}{\partial x} \equiv D_{i,z} \frac{\partial \langle C_{i,z}^0 \rangle}{\partial x} - \mu_{i,z} \langle C'^0_{i,z} E'^0 \rangle - \langle u'^0_b C'^0_{i,z} \rangle \quad (8)$$

The deviation terms for concentration, electric field, and bulk velocity are defined as $C'^0_{i,z} = C^0_{i,z} - \langle C^0_{i,z} \rangle$, $E'^0 = E^0 - \langle E^0 \rangle$ and $u'^0_b = u^0_b - \langle u^0_b \rangle$. Equations 5 and 6 describe the transient development of the LE−TE interface. The LE−TE interface is initially dispersed over a lengthscale d, and the characteristic time to steady state is $\tau = d/\mu_0 E_0$, where μ_0 and E_0 are the characteristic electrophoretic mobility and electric field scales. For a typical ITP experiment, $d \sim 100\ \mu$M, $\mu_0 \sim 1 \times 10^{-8}$ m^2/V s and $E_0 \sim 100$ V/cm, resulting in a characteristic evolution time $\tau \sim 1$ s. Background ions and electric field distributions therefore reach steady state quickly (~1 s) compared to the time scale over which sample preconcentration occurs (described by eq 7, ~100 s or more). We, therefore, first solve for the background species and electric field evolution over the short time scale. The steady state, zeroth order, area-averaged electric field $\langle E^0 \rangle$ solution (i.e., when the disturbance wave due to interface relaxation has moved out of the computational domain) is used to solve for the transient sample growth of the sample via eq 7. By decoupling these two transient processes, occurring over disparate time scales, we reduce the computational time for sample evolution to ~10 min compared to, for example, a 4−5 h run time for SIMUL.

While solving for the background species evolution, at each location and time step, we correct for the effect of ionic strength on the fully ionized mobility and pK_a of background electrolyte species using the Pitts equation[31] and the Truesdell−Jones[32] model (see relations in Supporting Information). The fully dissociated electrophoretic mobilities and pK_a of the LE and TE species were determined from the database available in SIMUL.[28] The electrophoretic mobility of Alexa-Fluor 488 was determined via on-chip electrokinetic injection in independent experiments in a homogeneous buffer. We also performed electrophoretic injections of Rhodamine B (a neutral marker) to quantify the electroosmotic flow. A plot of the mobility of Alexa Fluor as a function of ionic strength of the histidine-phenylpropionic acid solution (pH = 5.3) is given in the Supporting Information in Figure S-1. The diffusion coefficients of the species were determined from fully ionized mobility values using the Nernst−Einstein relationship. The effective dispersion coefficient ($D_{\text{eff},i}$) described in eq 8 is therefore the only unknown parameter in the model and is obtained semiempirically, as described later. Note $D_{\text{eff},i}$ is useful only in predicting the concentration profile of the analyte and is not required to predict the analyte accumulation rate and peak migration speed. We solve eqs 5–7 using MATLAB's partial differential equation solver PDEPE.

Analytical Model for Sample Accumulation Rate. We present analytical expressions for total moles and concentration of sample accumulated at the LE−TE interface for the peak-mode ITP regime. A summary of the analysis and results is presented here, while more details can be found in the Supporting Information. In this analysis, the leading and trailing electrolytes consist of weak, univalent acids/bases and the pH jump across the LE−TE interface is not significant. We here use the result inferred from the perturbation analysis earlier: namely, that dilute sample ions do not contribute substantially to the conductivity of the ITP zone. The composition of the TE zone consisting of weak univalent

(31) Robinson, R. A.; Stokes, R. H. *Electrolyte Solutions, the Measurement and Interpretation of Conductance, Chemical Potential, and Diffusion in Solutions of Simple Electrolytes*; Butterworth: Guilford, U.K. 1965.

(32) Truesdell, A. H.; Jones, B. F. *U.S. Geol. Surv.* **1974**, *2*, 233–248.

electrolytes can be readily obtained using Jovin's[17] and Alberty's[16] relations. The result has a form similar to that obtained using the Kohlrausch regulating function[15] for fully ionized species

$$C_T^{te} = C_L^{le}\frac{\mu_T^{te}}{\mu_L^{le}}\left(\frac{\mu_C^{le} + |\mu_L^{le}|}{\mu_C^{te} + |\mu_T^{te}|}\right) \tag{9}$$

where $|\mu|$ denotes the absolute value of electrophoretic mobility μ (signed quantity). The sample concentration in the regulated TE zone (where LE species have been displaced by TE) is related to the initial sample concentration in the well and the ratio of conductivities of the regulated TE zone and TE well:

$$C_S^{te} = \frac{\alpha_S^{te,well}\mu_s^{te,well}}{\alpha_S^{te}\mu_s^{te}}\frac{\sigma_{te}}{\sigma_{te,well}}C_S^{te,well} \tag{10}$$

where $\alpha_S^{te,well}$is the degree of dissociation of sample ions in the TE well (where the initial sample−TE mixture is loaded).

The accumulation rate of sample ions equals their net electromigration influx from the TE zone (in the frame moving with the interface) since the diffusive fluxes are important only within the interface, and therefore, $dN_S/dt = (\mu_S^{te}E_{te} - V_{ITP})C_S^{te}$ where E_{TE} is the electric field in the regulated TE zone and V_{ITP} is the isotachophoretic velocity of the LE−TE interface given by

$$V_{ITP} = \frac{\alpha_L^{le}\mu_L^{le}j}{\sigma_{le}} = \frac{\alpha_T^{te}\mu_T^{te}j}{\sigma_{te}} \tag{11}$$

On integrating the sample accumulation equation in time, substituting for C_S^{te}, and simplifying, we obtain the following expression of accumulated moles of sample ions at a distance x downstream of the initial LE−TE interface location

$$N_S = \frac{(\alpha_S^{te}\mu_S^{te} - \alpha_T^{te}\mu_T^{te})}{\alpha_L^{le}\mu_L^{le}}\frac{\alpha_S^{te,well}\mu_S^{te,well}}{\alpha_S^{te}\mu_S^{te}}\frac{\sigma_{le}}{\sigma_{te,well}}C_S^{te,well}x \tag{12}$$

Here we used the fact that V_{ITP} is constant and so $x = V_{ITP}t$, converting time to distance, x, along the separation channel. The analytical solution for the concentration profiles at the interface for fully ionized electrolyte species has been derived by Coxon et al.[33] On the basis of similar analysis, we obtain an estimate of the width of the interface of weak electrolytes, assuming the effective degree of dissociation of LE and TE ions do not change significantly across the interface.

$$w \approx \frac{2kT}{e}\frac{\alpha_L^{le} + \alpha_T^{te}}{\alpha_L^{le}\alpha_T^{te}}\frac{\alpha_T^{te}\mu_T^{te}}{(\alpha_L^{le}\mu_L^{le} - \alpha_T^{te}\mu_T^{te})}\frac{\sigma_{le}}{j} \tag{13}$$

Notably, we have verified that the width predictions from this expression agree very well with the complete numerical solution using SIMUL even when the pH jump across interface is almost 2 units. This shows the weak dependence of interface width on variations in the degree of dissociation across the interface.

Lastly, leveraging eqs 12 and 13, we obtain the concentration of sample species at the LE−TE interface,

$$C_S \approx \frac{N_S}{w} = K\frac{j}{\sigma_{te,well}}C_S^{te,well}x \tag{14}$$

where$K$ is a function of effective mobilities of LE, TE, and the sample species. Equations 12–14 show the influence of key parameters such as current density and TE and LE concentrations on the dynamics. They also provide an estimate of maximum analyte concentration in the absence of dispersion effects. As we shall discuss in the Results and Discussion section, this simple model provides an accurate estimate of the peak area (accumulated moles) and captures trends of the dependence of sample zone width and concentration on various experiment parameters fairly well. The main limitation of this analytical model is the absence of dispersion dynamics, and therefore, the predicted sample zone width and concentration differ from the experimental values by up to ∼2-fold.

EXPERIMENTAL SECTION

We performed controlled single interface ITP experiments to study the influence of the governing parameters on sample preconcentration and validate our theoretical model. We impose constant current conditions to maintain a constant electric field in the LE and TE zones over time. In all the experiments, we used histidine-HCl (500 mM stock solution, pH = 4.3) as the LE and 3-phenylpropionic acid (50 mM stock solution, titrated with NaOH to pH = 4.9) as the TE. We chose to perform these experiments at low-pH conditions to prevent interference due to focusing of carbonate ions (from dissolved, atmospheric carbon dioxide) at the LE−TE interface. We added 1% polyvinyl-pyrrolidone (PVP) to all solutions as a dynamic coating to suppress electroosmotic flow.[34] We chose Alexa-Fluor 488 (Invitrogen) as the model analyte due to its excellent photostability and pH insensitive fluorescence above pH 4.[35] We prepared 10 μM stock solutions of Alexa-Fluor 488 and diluted to a final concentration of 10 nM in the TE. All the experiments were performed in a Caliper NS-12A glass microchip with simple-cross geometry and wet-etched 90 μm wide and 20 μm deep channels.

We used an inverted epifluorescent microscope (IX70, Olympus, Hauppauge, NY) equipped with a mercury lamp, a U-MWIBA filter-cube from Olympus (460−490/505/515 nm) and a 10× (NA = 0.4) UPlanApo objective for fluorescence imaging. Images were captured using a 12 bit, 1300 × 1030 pixel array CCD camera (Coolsnap, Roper Scientific, Trenton, NJ) externally triggered using an Agilent function generator. We used two sourcemeters (Keitheley 2410, Cleveland, OH), computer-controlled with Labtracer 2.0, to run constant current experiments at high voltage (up to 2200 V). We connected their ground terminals, applied a fixed −1100 V with the first sourcemeter, and used the second sourcemeter in constant current mode. (We caution that the sourcemeter should not be connected to a standard power supply as this can damage the sourcemeter and become a safety hazard.)

ITP Protocol. The protocol schematic is shown in Figure 1. All channels are initially filled with LE by loading wells 1, 2, and 3, and applying vacuum on well 4. Well 4 is then rinsed with DI

(33) Coxon, M.; Binder, M. J. *J. Chromatogr.* **1974**, *95*, 133–145.

(34) Kaneta, T.; Ueda, T.; Hata, K.; Imasaka, T. *J. Chromatogr., A* **2006**, *1106*, 52–55.

(35) Panchuk-Voloshina, N.; Haugland, R. P.; Bishop-Stewart, J.; Bhalgat, M. K.; Millard, P. J.; Mao, F.; Leung, W. Y. *J. Histochem. Cytochem.* **1999**, *47*, 1179–1188.

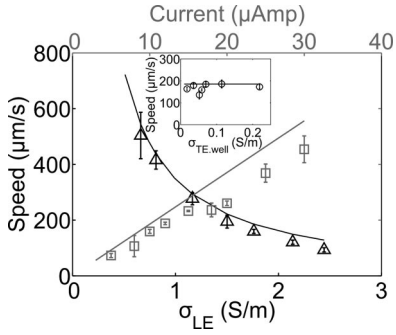

Figure 2. Speed of the analyte zone is plotted as a function of LE conductivity ($\sigma_{LE,well}$), current, and TE conductivity ($\sigma_{TE,well}$) (shown in inset). The three experimental parameters σ_{LE}, $\sigma_{TE,well}$, and current were varied independently. For the cases showing variation of speed with $\sigma_{LE,well}$ (△), the TE was 15 mM Na-phenylpropionic acid and the current was 10 μA. For cases showing dependence of speed on current (□), the TE was 15 mM Na-phenylpropionic acid and LE was 240 mM histidine-HCl. Finally, for dependence on $\sigma_{TE,well}$ (○), LE was 240 mM histidine-HCl and the current was 10 μA. The theoretical predictions of the ITP sample zone speed are shown as solid lines (with no fitting parameters).

water several times and loaded with the TE−analyte mixture. We note that the self-sharpening dynamics of ITP negates the need for on-chip electrokinetic injection procedures, and the well-to-channel interface is sufficient to achieve controlled and reproducible ITP interfaces. We then apply high voltage across wells 2 and 4 and acquire the image of the concentrated ITP sample zone at six locations downstream of the TE well by manually positioning the microscope stage. At each location, we obtained a set of 200 images, which were background corrected and normalized with flat-field images of the microchannel filled with 10 μM Alexa Fluor-488.[24] The normalized images are width-averaged and low-pass filtered with a two pixel standard deviation Gaussian kernel. We then use cross-correlations and ensemble averaging of these intensity measurements to obtain the average speed and axial concentration profiles of the sample zone. We estimate the width of the ITP sample zone by measuring the full width at half-maximum for this ensemble-averaged intensity profile.

RESULTS AND DISCUSSION

From our analytical expressions for sample accumulation rate and concentration (eqs 12 and 14), we find that sample zone dynamics in peak mode ITP are governed by current density j, LE and TE zone conductivity (σ_{le} and $\sigma_{te,well}$). We therefore systematically varied these key parameters independently in our experiments.

Speed and Width of Sample Zone and Inference of D_{eff}.. We first present results for the sample zone migration characteristics and zone width as these influence the focusing dynamics and the final concentration of the sample zone. Figure 2 shows the speed of the sample zone at station 6 (41 mm downstream of the TE well) as a function of current, σ_{le} and $\sigma_{te,well}$. The speed increases with higher current and lower LE zone conductivity, both of which result in higher electric field in the LE zone. TE conductivity does not influence the electric field and the migration speed. This agrees with the theory since, from eq 11, the speed of the ITP sample zone is equal to the speed of the leading ions (which is in turn governed by the electric field in the LE zone).

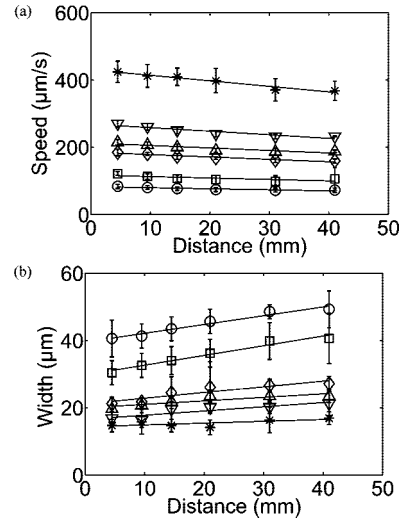

Figure 3. Plot of the speed and width of the sample zone at various locations downstream of the TE well. Shown are the speed and widths of the ITP sample zone for various constant current experiments: 5 (○), 8 (□), 10 (◇), 12 (△), 15 (▽) and 25 μA (∗). In all the cases, the leading and trailing electrolytes were 240 mM histidine-HCl and 15 mM Na-phenylpropionic acid, respectively. Linear regression fits are shown as solid lines.

Next, we analyze the speed and width of the sample zone as it migrates toward the LE well for constant current conditions. Figure 3a shows the speed of the sample zone versus location for various applied currents. Each data point denotes an average of five realizations and the error bars denote 95% confidence interval from the Student t distribution. The solid lines are linear regression fits to experimental data. The speed of the LE−TE interface is governed by the electric field in the leading zone and is expected to remain constant under constant current conditions (also seen from eq 11). However we observe slight reduction in the sample zone speed with distance (speed at $x = 5$ mm is ∼10% higher than that at $x = 41$ mm). This slight decrease in speed is attributable to a residual level of EOF remaining despite aggressive EOF suppression with 1% PVP dynamic coating. The TE zone has lower conductivity than the LE, resulting in higher local electric field (and likely slightly higher residual EOF mobility). Assuming that the EOF mobility does not differ significantly in the LE and the TE zones, we can derive a simple relation for variation of the average EOF velocity as the sample zone migrates distance x downstream from the TE well.[36]

$$\overline{V_{eof}} = \frac{\varepsilon\zeta\overline{E}}{\eta} = \frac{\varepsilon\zeta E_{le}}{\eta}\left(\left(\frac{\alpha_L\mu_L}{\alpha_T\mu_T} - 1\right)\frac{x}{L} + 1\right) \qquad (15)$$

Here ε is the permittivity, ζ is the average zeta potential, η is the viscosity of the solution, and L is the total length of the microchannel. We therefore expect a linear increase in average EOF and decrease in net speed of the sample zone as it migrates, also seen in Figure 3a.

Next, we discuss the variation of the width of the ITP interface (as quantified by the width of this "peak mode" sample zone) with distance for various values of current, as summarized in Figure

(36) Herr, A. E.; Molho, J. I.; Santiago, J. G.; Mungal, M. G.; Kenny, T. W.; Garguilo, M. G. *Anal. Chem.* **2000**, *72*, 1053–1057.

3b. We observe a slight, linear increase in the width of the sample zone as it migrates over ~45 mm length. This linear increase is in contrast to the constant interface width predicted by the theoretical models to date, which do not account for dispersion effects.[27,28] To our knowledge, Saville's study[37] on effect of EOF on the structure of ITP boundaries has been the only attempt at studying dispersion effects in ITP. Saville's Taylor analysis of the ITP boundary does not agree well with our experiments, most likely because it assumed a locally uniform, induced parabolic flow due to the EOF mismatch leading to axial dispersion that is balanced by radial diffusion. In contrast, typical ITP flow fields are fully three-dimensional near the interface with strong velocity and electric fields gradients[38] that induce transverse mixing.

We employ a simple, semiempirical approach to quantifying dispersion at the ITP interface under conditions of reduced EOF (and no externally applied pressure gradients). From Figure 3a,b, we observe that both EOF velocity and the width of the sample zone increase linearly with distance x from the TE well. This provides evidence of a linear relationship between the sample zone width and EOF velocity. The induced pressure gradient, created due to EOF mismatch, distorts the ITP interface (the term $\langle u_b'^0 C_{i,z}'^0 \rangle$ in eq 8) and generates transverse electric field gradient in the vicinity of the interface. From our experiment observations of the ITP interface scalar fields, we hypothesize that the transverse electromigration flux in the distorted interface region balances axial dispersion. We perform scaling analysis of the balance of axial dispersion and transverse electromigration (presented in Supporting Information) and arrive at an effective dispersion coefficient of the form $D_{\text{eff}} = D_i(1 + \beta \overline{V_{\text{eof}}}\, a/D_i)$; where $\overline{V_{\text{eof}}}$ is the average electroosmotic velocity and a is a characteristic channel dimension (channel width in this case).[39] β here scales as $[(E_x/E_y)(\mu_L - \mu_T)/\mu_T]$, where E_x and E_y are the axial and transverse electric field components in the interface region, and is used as a fitting parameter to predict dispersion. By minimizing the error between the theoretical sample zone width and the experimentally observed widths, we estimate $\beta = 2$. This single value of β can be used to quantitatively predict dynamics of the sample zone axial distribution, across changes in LE, TE, and j.

Figure 4a,b show data for the sample zone width as a function of current, LE, and TE conductivities. We observe narrower peak width for high current density and for low LE conductivity conditions. In peak-mode ITP, the interface width (also, sample zone width) is governed by the balance of dispersion and electromigration fluxes of the leading ion, trailing ion, and counter ion. Under higher electric field (high j and low σ_{LE}), the electromigration flux increases and the interface sharpens. Again the TE buffer conductivity ($\sigma_{te,well}$) does not influence the electric field, and therefore, the width of the ITP sample zone, as is seen in the inset of Figure 4a. The solid line, dashed line, and dashed−dotted line, respectively, represent the predicted sample width using our proposed dispersion model, Saville's Taylor dispersion model, and the analytical model of eq 13 above. Dispersion accounts for a ~2-fold widening of the interface, and the Taylor dispersion model deviates from observed trends under high electric field conditions.

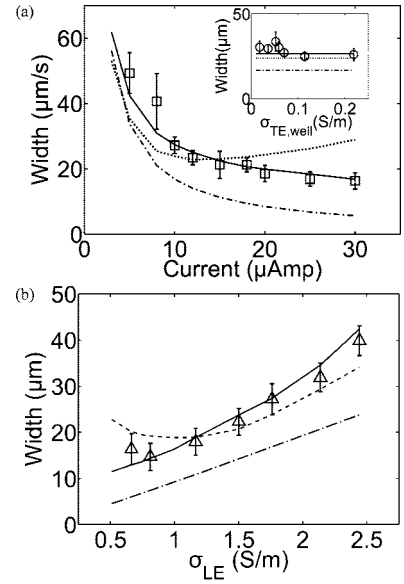

Figure 4. Plots of the ITP sample zone width as a function of current, LE conductivity (σ_{LE}), and TE conductivity ($\sigma_{TE,well}$) (shown in inset). The experiment conditions for each case are given in the caption of Figure 2. The prediction of the width using our dispersion model (with fitting parameter $\beta = 2$) is shown with a solid line. As a comparison, predictions from a simple Taylor dispersion model (with D_{eff} assumed to have the form $D_{\text{eff}} = D_0(1 + 6/210Pe^2)$, where $Pe = V_{\text{eof}}a/D_0$) are shown with a dotted line. Predictions from the (pure diffusion) analytical model are shown with a dashed−dotted curve, respectively.

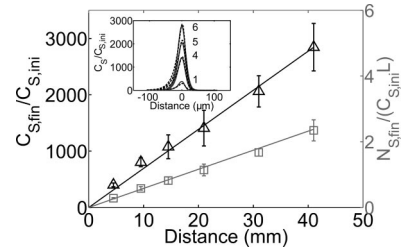

Figure 5. Plot of the analyte concentration ($C_{S,fin}$) and accumulated moles of analyte ($N_{S,fin}$), nondimensionalized with initial concentration ($C_{S,ini}$) and channel length (L), at various locations downstream of the initial LE−TE interface location. Here, the leading and trailing electrolytes were 240 mM histidine-HCl and 15 mM Na-phenylpropionic acid, respectively, and current was held constant at 10 μA. Predictions of $C_{S,fin}$ and $N_{S,fin}$ with the perturbation model are shown as a black and gray solid line, respectively. The inset plot shows the concentration profile of the analyte at stations 1, 4, 5, and 6 as a function of relative axial distance from the peak. The theoretical predictions of concentration profiles from the perturbation analysis are shown as dashed curves.

Sample Accumulation and Concentration. Peak area quantifies the accumulated moles of sample and is a critical figure of merit in determining signal strength and sensitivity. It also determines extraction efficiency in ITP-based fractionation assays. Typical plots of total amount and the concentration of analyte accumulated in the sample zone at various locations downstream of the TE well for the constant current ITP experiment are shown in Figure 5. The current was held constant at 10 μA and the voltage increased linearly from 214 to 740 V as the sample zone

(37) Saville, D. A. *Electrophoresis* **1990**, *11*, 899–902.
(38) Bharadwaj, R.; Santiago, J. G. *J. Fluid Mech.* **2005**, *543*, 57–92.
(39) This form of the dispersion coefficient is different than the typical form of Taylor dispersion analyses. However, we do not expect typical Taylor dispersion analyses to apply here as field gradients are highly three-dimensional and interface widths are on the order of channel width. (ref 38).

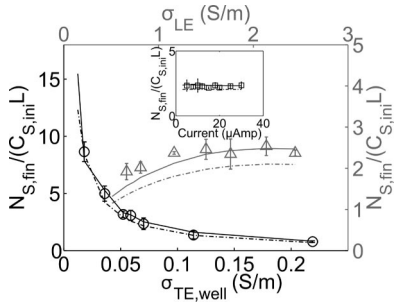

Figure 6. Plot of accumulated moles of analyte ($N_{S,fin}$) in the sample zone at $x = 41$ mm, nondimensionalized with initial concentration ($C_{S,ini}$) and channel length (L), as a function of LE conductivity (σ_{LE}, △), TE conductivity ($\sigma_{TE,well}$, ○) and current (□) (shown in inset). The experiment conditions for each case are given in the caption of Figure 2. The solid curve and the dashed−dotted curve indicate the theoretical estimate of total accumulated sample obtained from the perturbation model and the analytical model, respectively.

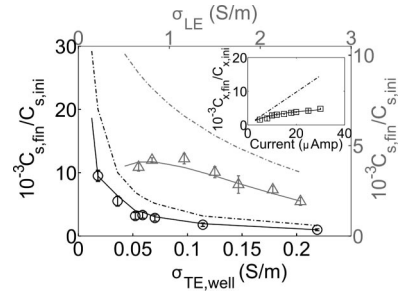

Figure 7. Plot of the analyte concentration ($C_{S,fin}$) at $x = 41$ mm, nondimensionalized with initial concentration ($C_{S,ini}$) as a function of LE conductivity (σ_{LE},△), TE conductivity ($\sigma_{TE,well}$,○) and current (□) (shown in inset). The experiment conditions for each case are given in the caption of Figure 2. The theoretical prediction from the perturbation analysis model and the analytical model are shown in the solid and dashed−dotted curves, respectively. The gray and black lines indicate the appropriate plot axis.

migrated from $x = 0$ to 41 mm. In Figure 5, we plot the total moles of sample accumulated per unit cross-section area ($N_{S,fin}$), nondimensionalized with initial sample concentration ($C_{S,\ ini}$) and channel length (L). The peak area and height both increase linearly with distance. These data show accumulated sample does not influence the local electric field, and hence, our perturbation analysis is valid. Further, these data show that the influx of sample ions into the sample zone under constant current conditions remains unchanged, resulting in a linear increase in moles of accumulated sample. The sample concentration also increases linearly since the width of the ITP interface increases gradually (∼15% increase in width over the 41 mm distance). The perturbation model predictions for peak area and sample concentration are shown with dashed curves. The peak area prediction has no fitting parameter, and sample concentration uses only the empirical $\beta = 2$ for all cases. We also show measured sample concentration profiles at station 1, 4, 5, and 6 versus predicted concentration profiles in the inset of Figure 5.

In Figure 6, we show the effect of the LE, TE conductivity, and current density (j) on peak area measured at station 6 ($x =$ 41 mm). First, from the plot in the inset of Figure 6, we observe that the current density does not influence the amount of sample accumulated for a given distance to the detector. This result also follows from eq 12. For these measurements, we varied the current from 5 to 30 μA and fixed the LE and TE concentrations to 240 mM histidine-HCl and 15 mM Na-PPa. At low j, accumulation rates are lower but the sample takes longer to reach a given distance. At higher j, the sample zone migrates at higher velocity, but the accumulation rate is proportionally increased, so it is therefore independent of j. This is an important consideration in the placement of detectors and optimizing the preconcentration duration in ITP-CE assays.

The main section of Figure 6 shows the effect of TE and LE composition on the moles of accumulated sample. In the top horizontal axis, we varied LE concentration from 80 to 350 mM (conductivity 6.62 to 24.4 mS/cm), maintaining the current at 10 μA and the TE concentration at 15 mM Na-PPa. The sample accumulation initially increases with the increasing LE concentration (up to 150 mM LE) and subsequently plateaus at higher concentration. The sample concentration in the regulated TE zone, and therefore the accumulation rate, increases with the LE concentration. At higher LE concentration, the peak area asymptotes due to the influence of ionic strength on the electrophoretic mobilities of species. At the given conditions, the multivalent sample ions experience greater retardation at high ionic strength than the univalent leading and trailing ion. As a result, for higher LE concentration (higher ionic strength), the difference between the sample and the TE mobility reduces so that the difference ($\alpha_S^{te}\mu_S^{te} - \alpha_T^{te}\mu_T^{te}$) in eq 12 decreases, resulting in a reduced influx of sample ions into the sample zone.

The bottom horizontal axis of Figure 6 shows the influence of the TE zone conductivity on sample accumulation. We increased the conductivity of the TE solution in well 1 from 0.18 to 2.19 mS/cm (TE composition: 2.5−34 mM Na and 15−50 mM PPA). Here LE concentration was maintained at 240 mM histidine-HCl, and the current was held constant at 10 μA. The peak area scales approximately as $1/\sigma_{te,well}$ and therefore reduces by ∼10-fold. As the initial TE conductivity is lowered, the electric field in the TE well increases, which results in a higher influx of sample ions into the LE−TE interface. This trend is again predicted by eq 12 which gives an expression for moles of accumulated sample at a given distance from the initial interface location. We note that the solid lines in Figure 6 are predictions from the perturbation model and dashed lines are predictions from the analytical model. There is again excellent quantitative agreement between the models and experiments.

Lastly, we present an investigation of the dependence of the preconcentration ratio, $C_{S,fin}/C_{S,ini}$, on current, LE, and TE conductivity. First, as seen in the inset in Figure 7, the preconcentration ratio initially increases linearly with current and plateaus at higher current values. The concentration of accumulated sample at the LE−TE interface $C_{S,fin}$ scales as the ratio of moles of sample accumulated (N_S) to the width of the interface (δ). Again, from eqs 12 and 13, the peak area is not influenced by the current density but the interface width scales inversely with current density. At high current conditions, dispersion effects begin to dominate and so the interface width δ does not reduce inversely with applied current (cf. Figure 5). As a result, the preconcentration ratio plateaus at higher current density. Also, from Figure 7, the sample concentration follows the same inverse dependence on TE conductivity (σ_{TE}) as the peak area. This result also follows from the previous results of the influence of σ_{TE} on the interface

width and peak area. σ_{TE} does not affect the interface width but results in a higher peak area (N_S) for low σ_{TE}. The upper curve in Figure 7 shows the dependence of the preconcentration ratio on LE conductivity. Here we observe an optimum LE conductivity (~8 mS/cm, 100 mM histidine-HCl) at which the sample preconcentration ratio is maximum. This is expected as higher σ_{LE} results in higher peak area and also higher interface width (both increase nonlinearly). The experimental data presented here agrees well with our perturbation model, while the analytical model capture trends but overpredicts the concentration 2−3-fold as it neglects dispersion effects.

CONCLUSION

We have presented a theoretical model and experimental study of sample preconcentration dynamics of commonly applied peak mode isotachophoresis. All ITP preconcentration assays with trace analyte concentrations operate in this regime, and ITP focusing results in approximately Gaussian shaped analyte zone peaks. Since the sample zone is confined within the adjacent LE−TE interface, accurate modeling of this regime requires well resolved ITP interfaces and accounting of dispersion effects. We apply regular perturbation analysis to this ITP problem to reduce the numerical stiffness of the governing equations and conclude that the sample species in peak mode merely respond to the electric field set up by the background LE and TE species. We use a semiempirical dispersion model to estimate the width of the ITP boundary, and this treatment accurately captures the observed trends in the experiments. We also present a closed-form analytical model that yields further intuition, at the expense of not accurately capturing the ITP interface width. The latter analytical model identifies key parameters governing preconcentration dynamics and bounds the maximum achievable values of preconcentration ratio and peak analyte concentration given perfect suppression of EOF (i.e., negligible dispersion). We validated our perturbation and analytical models with a detailed parametric study including variations in current density, LE concentration, and TE concentration.

The study identifies conditions required to achieve high sample accumulation rate and concentration increase. For example, low TE concentration achieves high accumulation rate, and the amount of accumulated sample depends on the position of the sample zone but not current density. High current density results in higher preconcentration ratio, as the interface sharpens with increasing current. In contrast, increasing LE concentration results in higher sample concentration in the regulated TE zone and therefore higher accumulation rate, but at the expense of a wider sample zone width since high LE concentration also lowers the electric field in the LE zone. These trends combine to give a critical LE concentration at which maximum preconcentration is obtained. The latter is contrary to predictions from traditional ITP theory (e.g., based on KRF). Overall, the study provides useful guidelines for designing ITP experiments and yields physical insight into the preconcentration dynamics.

ACKNOWLEDGMENT

This work is sponsored by the National Institutes of Health (Grant N01-HV-28183). The authors thank Rob Chambers and Moran Bercovici for insightful discussions regarding the physics of dispersion in ITP.

SUPPORTING INFORMATION AVAILABLE

CCD images of the sample zone, mobility of Alexa-Fluor 488 as a function of ionic strength, perturbation analysis and area-averaging of species transport equations, analytical solution of sample concentration growth at the LE−TE interface, corrections for electrophoretic mobility and activity coefficient, and scaling analysis of the effective dispersion coefficient. This material is available free of charge via the Internet at http://pubs.acs.org.

Received for review April 21, 2008. Accepted June 3, 2008.

AC800792G